



# Simultaneous whole-body and breast <sup>18</sup>F-FDG PET/MRI examinations in patients with breast cancer: a comparison of apparent diffusion coefficients and maximum standardized uptake values

Michiro Sasaki<sup>1</sup> · Mitsuhiro Tozaki<sup>2</sup> · Kazunori Kubota<sup>3</sup> · Wakana Murakami<sup>4</sup> · Daisuke Yotsumoto<sup>5</sup> · Yasuaki Sagara<sup>5</sup> · Yasuyo Ohi<sup>6</sup> · Shunichi Oosako<sup>7</sup> · Yoshiaki Sagara<sup>2</sup>

Received: 19 July 2017 / Accepted: 12 November 2017

© Japan Radiological Society 2017

## Abstract

**Purpose** To compare standardized uptake value (SUV) and apparent diffusion coefficient (ADC) values acquired using a PET/MRI scanner in breast cancer patients.

**Materials and methods** Whole-body PET/MRI and breast PET/MRI were performed in 108 consecutive patients. Ninety-four patients who had a total of 100 breast cancers were analyzed. SUVmax and ADCmean acquired using breast PET/MRI were compared with pathologic prognostic factors.

**Results** All the lesions were visually detectable using PET and diffusion-weighted imaging (DWI) on breast PET/MRI; however, lesions were visually undetectable on whole-body DWI in 13 patients (13%) or on whole-body PET in 7 patients (7%). An analysis of ADCmean and SUVmax demonstrated a statistically significant correlation between whole-body imaging and breast imaging ( $\rho = 0.613$ ,  $p < 0.001$  and  $\rho = 0.928$ ,  $p < 0.001$ , respectively). In a univariate analysis, SUVmax was significantly correlated with HER2 status ( $p < 0.001$ ), Ki-67 ( $p = 0.014$ ), tumor size ( $p = 0.0177$ ), and nuclear grade ( $p = 0.0448$ ). In multiple regression analysis, only tumor size ( $p = 0.00701$ ) was shown to independently influence SUVmax.

**Conclusion** Prone breast imaging was more sensitive than whole-body PET/MRI for detection of breast cancers. Both SUVmax and ADCmean showed limited correlation with pathologic prognostic factors.

**Keywords** PET/MRI · Standardized uptake value · Apparent diffusion coefficient · Diffusion-weighted imaging · Breast carcinoma

## Introduction

The integration of a positron emission tomography (PET) component within an MR-scanner has provided a new generation of multi-modal imaging, combining functional PET data with structural and functional information obtained

from MRI. PET/MRI has a number of advantages, such as improved soft-tissue contrast, the possibility of performing truly simultaneous instead of sequential acquisitions, and the availability of sophisticated MRI sequences, such as diffusion and perfusion imaging, functional MRI, and MR spectroscopy, which can provide important information [1].

✉ Michiro Sasaki  
chacha622@sagara.or.jp

<sup>1</sup> Department of Radiology, Sagara Perth Avenue Clinic, 26-13 Shinyashiki-cho, Kagoshima, Kagoshima 892-0838, Japan

<sup>2</sup> Department of Radiology, Sagara Hospital Affiliated Breast Center, 3-28 Tenokuchi-cho, Kagoshima, Kagoshima 892-0845, Japan

<sup>3</sup> Department of Medical Informatics, Tokyo Medical and Dental University Hospital, 1-5-45 Yushima, Bunkyo-ku, Tokyo 113-8519, Japan

<sup>4</sup> Department of Radiology, National Defense Medical College, 3-2 Namiki, Tokorozawa, Saitama 359-0042, Japan

<sup>5</sup> Department of Breast Surgery, Sagara Hospital, 3-31Mtsubara-ch, Kagoshima, Kagoshima 892-0833, Japan

<sup>6</sup> Department of Pathology, Sagara Hospital, 3-31Mtsubara-cho, Kagoshima, Kagoshima 892-0833, Japan

<sup>7</sup> Image Inspection Department, Sagara Perth Avenue Clinic, 26-13 Shinyashiki-cho, Kagoshima, Kagoshima 892-0838, Japan

Recently, PET/MRI has emerged as a new tool with significant clinical potential for the evaluation and management of cancer patients [2–8]. Moreover, data suggest that PET/MRI findings might have a larger impact on oncologic management decisions than PET/CT findings [9–12]. These properties make this modality an excellent potential tool for the staging of patients with breast cancer.

Meanwhile, whole-body diffusion-weighted imaging (DWI) has recently received considerable attention worldwide and has been reported as a useful tool in pre- and post-operative cancer patients requiring follow-up examinations to check for metastasis [9, 13, 14]. Furthermore, breast DWI studies show significantly lower apparent diffusion coefficient (ADC) values in malignant tumors than in normal tissue or benign breast lesions, and improve the specificity of dynamic contrast-enhanced MRI [15–18]. Breast DWI is also useful for assessing the tumor's response to treatment.

FDG-PET and DWI are both functional modalities that indirectly represent the biological characteristics of breast cancer. In addition, there are many studies exploring the association between the two modalities and prognostic factors. However, most of the published papers comparing the standardized uptake value (SUV) versus the ADC value in breast cancer patients describe comparisons made using PET/CT and MRI [19–24]. For a more accurate comparison of SUV<sub>max</sub> versus ADC<sub>mean</sub>, data generated using a PET/MRI scanner, enabling simultaneous imaging of the same anatomic site, are thought to be necessary.

The aim of the present study was to compare SUV<sub>max</sub> and ADC<sub>mean</sub> values acquired using breast imaging with a PET/MRI scanner directly in the same patients with breast carcinoma. In addition, we assessed the correlations between SUV<sub>max</sub> and ADC<sub>mean</sub> acquired using whole-body PET/MRI in a supine position (SUV-whole body and ADC-whole body) as well as the correlations between SUV and ADC values acquired using breast PET/MRI in a prone position (SUV-breast and ADC-breast) for the evaluation of breast cancer. Finally, we compared the SUV-breast and ADC-breast findings with pathologic prognostic factors.

## Materials and methods

### Patients

This retrospective study was approved by our institutional review board. All the patients provided written informed consent for the review of their medical records and images.

Between October 2016 and February 2017, whole-body PET/MRI in a supine position and breast PET/MRI in a prone position were performed for preoperative evaluations in 108 consecutive patients at our hospital. Fourteen patients who did not undergo surgery ( $n = 9$ ) or who were evaluated

after receiving chemotherapy ( $n = 5$ ) were excluded. The remaining 94 patients (age range, 24–84 years; mean, 59 years) who had a total of 100 breast cancers were analyzed in this study.

### Imaging protocol

Patients fasted for at least 4–6 h before the intravenous administration of 18F-FDG with average radioactivity of MBq (3.7 MBq/kg of body weight; range, 122.0–233.4 MBq).

First, a supine whole-body PET/MR scan was performed 60–100 min after the injection of 18F-FDG, covering a field of view from the parietal region to the mid thighs. After whole-body PET/MR was completed, breast PET/MRI was performed with the patients in the prone position; the scan was started approximately 90–130 min after the injection.

The integrated PET/MR scanner (Biograph mMR; Siemens Healthcare GmbH, Erlangen, Germany) consisted of a 3-T MR system and an inline PET system with an avalanche photodiodes (APD) detector. The APD are not only insensitive to a magnetic field but also have a small space to be cased within the MR gantry. The PET unit has an axial field of view of 25.8 cm and offers the advantage of fewer bed positions in a short time. The PET data were reconstructed using a 3-dimensional (3D) ordinary Poisson ordered-subsets expectation maximization with a point spread function algorithm with 2 iterations and 21 subsets ( $172 \times 172$  matrix, zoom 1, slice thickness 2 mm). A post-reconstruction Gaussian filter with 4.0 mm full-width at half maximum was applied. An MRI-based attenuation correction of the PET data was accomplished according to the method described by Martinez-Moller et al. [25]. The imaging protocol was designed with reference to the study by Martinez-Moller et al. [26]. Whole-body PET/MR was performed in a caudocranial direction, with a total imaging matrix (Tim) coil. The Tim coil is an approved surface coil for PET/MR, which improves image quality and reduces imaging time with MRI, similar to that in standalone MRI. After acquisition of the initial T1-weighted two-point Dixon 3D volumetric interpolated breath-hold examination (VIBE) for attenuation correction, axial T1-weighted VIBE and axial T2-weighted half-Fourier single-shot turbo spin-echo (HASTE) sequences and axial diffusion weighted imaging (DWI;  $b = 0$ ,  $b = 800$ ) were obtained during simultaneous PET acquisition. Four to five PET bed positions were usually required, depending on the patient's height and the emission time per bed was 4 min.

The breast PET/MRI comprised a breast PET scan of one bed position and a simultaneous breast MRI using a standard 4-channel breast coil. The emission time of the PET scan was 15 min. The breast MRI examination consisted of a localizer sequence, coronal T1-weighted turbo spin-echo,

and sagittal T2-weighted fat-suppressed turbo spin-echo sequence, coronal a single-shot echo planar diffusion-weighted sequence (DWI;  $b = 0$ ,  $b = 1000$ ), and 3D dynamic contrast-enhanced (DCE) sequence. DCE-MRI was performed with coronal T1-weighted fat-suppressed 3D VIBE, with 1 pre-contrast and 3 post-contrast dynamic series performed within 5 min depending on the breast thickness after bolus injection. Next, 1 ml/s of gadobutrol (0.1 mmol/kg of body weight, Gadovist; Bayer Schering Pharma, Berlin, Germany) was injected, followed by a 20-ml saline flush. The detailed protocol used for whole-body PET/MR and breast PET/MR using the integrated PET/MR scanner is listed in Table 1.

### Image analysis

The analysis of whole-body PET/MR and breast PET/MR images was performed by two experienced radiologists. The PET and MR data sets were retrospectively analyzed on the PET/MR workstation (syngo.via; Siemens Healthcare GmbH) by using software (MR oncology and MR BreVis; Siemens Healthcare GmbH).

### Whole body PET/MRI

The PET images were evaluated visually and quantitatively by one experienced radiologist (M.S.) with 24 years of experience and one experienced nuclear medicine physician as well as an experienced radiologist (K.K.) with 18 years of experience with knowledge of the clinical information and the presence of breast carcinoma. For quantitative analysis of FDG uptake, a volume of interest (VOI) was placed over the most intense area of FDG accumulation by the primary breast tumor for each patient. PET scans with focally marked increased FDG uptake were considered definite. Moreover, the cases with diffuse or slight to moderate focally increased FDG uptake were considered positive to represent malignant tissue. The SUV was calculated as:  $SUV = VOI \text{ radioactivity concentration (Bq/ml)} / [\text{injected dose (Bq)} / \text{patient's weight (g)}]$ . SUVmax, which was defined as the highest SUV in the pixel with the highest count within the VOI, was measured and recorded for the focal areas of uptake.

The ADC value was calculated according to the formula:  $ADC = [1/(b_2 - b_1)] \ln (S_1/S_2)$ , where  $S_1$  and  $S_2$  are the signal intensities in the ROI obtained by two gradient factors,  $b_2$  and  $b_1$  ( $b_1 = 0$  and  $b_2 = 800 \text{ s/mm}^2$ ). For the measurement of the ADC value, one radiologist (M.S.) placed a region of interest (ROI) within the tumor on the ADC map by referring to the solid portion of T1WI, T2WI and fusion imaging, according to the methods published previously [21]. The ROIs were carefully placed inside the tumor avoiding the cystic portion or any visual artifact, and the mean ADC values within each ROI were recorded. We

calculated the average of the mean ADC values for all ROIs within the tumor.

### Breast PET/MRI

The PET image and MR image of the breast was analyzed by using the same method as that of whole-body PET analysis. The ADC value was calculated according to the formula:  $ADC = [1/(b_2 - b_1)] \ln (S_1/S_2)$ , where  $S_1$  and  $S_2$  are the signal intensities in the ROI obtained by two gradient factors,  $b_2$  and  $b_1$  ( $b_1 = 0$  and  $b_2 = 1000 \text{ s/mm}^2$ ). SUVmax and ADC values of MR imaging were measured for each individual tumor by referring to the enhancing solid portion of DCE-MRI. The findings of DCE-MRI were analyzed with MR BreVis software.

For the DCE-MRI analysis, subtraction images were generated by subtracting the pre-contrast images from all contrast-enhanced images. Subsequently, the tumor size, morphologic pattern (shape, margin, and internal enhancement of the mass lesion) during the early phase, and kinetics (percentage signal intensity increase during the early phase and kinetic curve type during the delayed phase) were evaluated for each lesion according to the Breast Imaging Reporting and Data System MRI guidelines [27].

### Histologic analysis

Pathologic reports were reviewed to determine the size, lymph node metastasis, and histologic grade. Immunohistochemistry was used to test for the expression of the following molecular markers: estrogen receptor (ER), progesterone receptor (PgR), human epidermal growth factor receptor 2 (HER2), and Ki-67. ER and PgR positivity was defined as the presence of 10% or more positively stained nuclei in ten high-power fields. Tumors with 2+ or 3+ scores were classified as HER2 positive, and tumors with 0 or 1+ were negative. Ki-67 of  $\geq 14\%$  was considered positive expression.

### Statistical analysis

The statistical analyses were performed with R statistical software, version 3.4 [28]. A  $p$  value of  $< 0.05$  was considered statistically significant. Data are presented as the mean values and range for continuous variables and as the frequency with percentage for categorical variables. The relationships between SUVmax, ADCmean values, and the clinicopathological parameters were calculated using the Mann–Whitney  $U$  test (for two groups). In addition, variables were subjected to multiple linear regression analysis to determine those that were independently associated with SUVmax or ADCmean. To evaluate the correlation between SUVmax and ADCmean, Spearman's correlation coefficient was calculated. To calculate optimal cutoff values of

**Table 1** Technical parameters for different MRI sequences

Sequence	TR (ms)	TE (ms)	FA (degree)	Turbo factor/EPI factor	B-value (s/mm <sup>2</sup> )	FOV (mm)	Matrix (read × phase)	Slice thickness (mm)/dist. factor (%)	Slices/slice per slab	PAT Sat.	Ave. Band width (Hz/pixel)	TA
<b>Whole body PET/MR</b>												
MRAC coronal	4	1.23	9.0	–	–	500	–	3.12	128	2	1	0:17
Dixon VIBE												
DWI axial	10,900	74	–	112	800	450	128 × 112	6.5/0	30	2	2	2:01
T1WI axial	4.1	1.23	9	–	–	450	320 × 190	4.1/20	48	2	1	0:15
FLASH		2.46										
T2WI axial	570	84	120	250	–	450	384 × 250	6.5/0	30	2	1	0:17
<b>Breast PET/MR</b>												
MRAC coronal	4	1.23	9.0	–	–	500	192 × 90	3.12	128	2	1	0:17
Dixon VIBE												
T2WI TSE	5210	61	120	18	–	200	256 × 205	2.5/20	39	2	1	2:05
DWI coronal	13,000	79	–	86	1000	340	148 × 86	3/10	40	2	3	3:15
T1WI coronal	135	2.46	69	–	–	340	384 × 230	3/10	40	2	1	1:06
T2WI coronal	4400	76	120	17	–	340	384 × 261	3/10	40	2	1	3:05
Dynamic T1WI coronal	3.68	1.38	10	–	–	360	448 × 278	0.9/20	160	2	1	1:00
T1WI sagittal	6.93	3.27	10	–	–	200	352 × 204	1.3/20	104	2	1	1:00
T1WI coronal	3.39	1.3	12	–	–	360	416 × 250	1.5/20	192	–	1	2:15

TR repetition time, TE echo time, FA flip angle, FOV field of view, PAT parallel acquisition techniques, Sat. saturation, Ave. average, TA acquisition time, SPAIR spectral attenuated inversion recovery, STIR short T1 inversion recovery, Water excit. water excitation, Q-fat sat. quick fat saturation, MRAC magnetic resonance attenuation correlation, EPI echo planar imaging, VIBE volume interpolated breath-hold examination, DWI diffusion-weighted imaging, FLASH fast low-angle shot, HASTE half Fourier acquisition single shot turbo spine echo, TSE turbo spin echo

SUVmax and ADCmean for statistically significant parameters and their sensitivity and specificity, receiver operating characteristic (ROC) curves were obtained based on the values of SUVmax and ADCmean. Based on these ROC curves, corresponding areas under the curve (AUC) were calculated.

## Results

### Histopathology

All 94 patients with a malignant biopsy result underwent a mastectomy or breast-conserving surgery. The histologic types of malignancy included ductal carcinoma in situ (DCIS) ( $n = 17$ ); invasive ductal carcinoma, not otherwise specified (ductal NOS) ( $n = 70$ , papillotubular carcinoma in 16, solid-tubular carcinoma in 14, scirrhous carcinoma in 40); invasive lobular carcinoma ( $n = 8$ ); mucinous carcinoma ( $n = 4$ ); and apocrine carcinoma ( $n = 1$ ).

The average size of the invasive tumors was 28.5 mm (range, 8.0–80 mm), while that of the DCIS lesions was 29.4 mm (range, 5.0–80 mm). According to the histological grade, 47 tumors were nuclear grade 1, and 36 tumors were grade 2 or 3. Axillary lymph node metastasis was found in 20 patients. Immunohistochemical findings showed 77

ER-positive tumors, 66 PgR-positive tumors, 8 HER2-positive tumors, and 39 Ki-67-positive tumors.

### Visual assessment of DWI and PET imaging

All the lesions were visually detectable using PET and DWI on breast PET/MRI (Fig. 1). Thus, the ADC and SUV could be determined for all the patients while referring to the DCE-MRI findings (Table 2).

Using whole-body PET/MRI, some lesions were difficult to identify visually, and the SUV could not be determined in 7 lesions (7%) (Table 2). Histopathologically, the tumors were identified as scirrhous carcinoma in 5 of these 7 lesions, papillotubular carcinoma in 1, and DCIS in 1 (Table 3). The average size of these lesions was 19.3 mm (range: 5–60 mm). The proportion of scirrhous carcinoma

**Table 2** Visual assessment of diffusion-weighted imaging and PET imaging

	Whole body		Breast imaging	
	Negative	Positive	Negative	Positive
DWI	13	87	0	100
PET	7	93	0	100

**Fig. 1** Whole-body PET/MR images (a, b, c), and breast PET/MR images (d, e, f) of a 65-year-old patient with invasive lobular carcinoma of the right breast. The lesion has high signal in axial (a) and coronal DWI (d). It is associated with a moderate focal uptake of  $^{18}\text{F}$ -FDG on PET images (b, e). Fusion of PET data and water-weighted Dixon MR data (c), coronal DCE-T1W fat saturated data (f) acquired on hybrid PET/MR

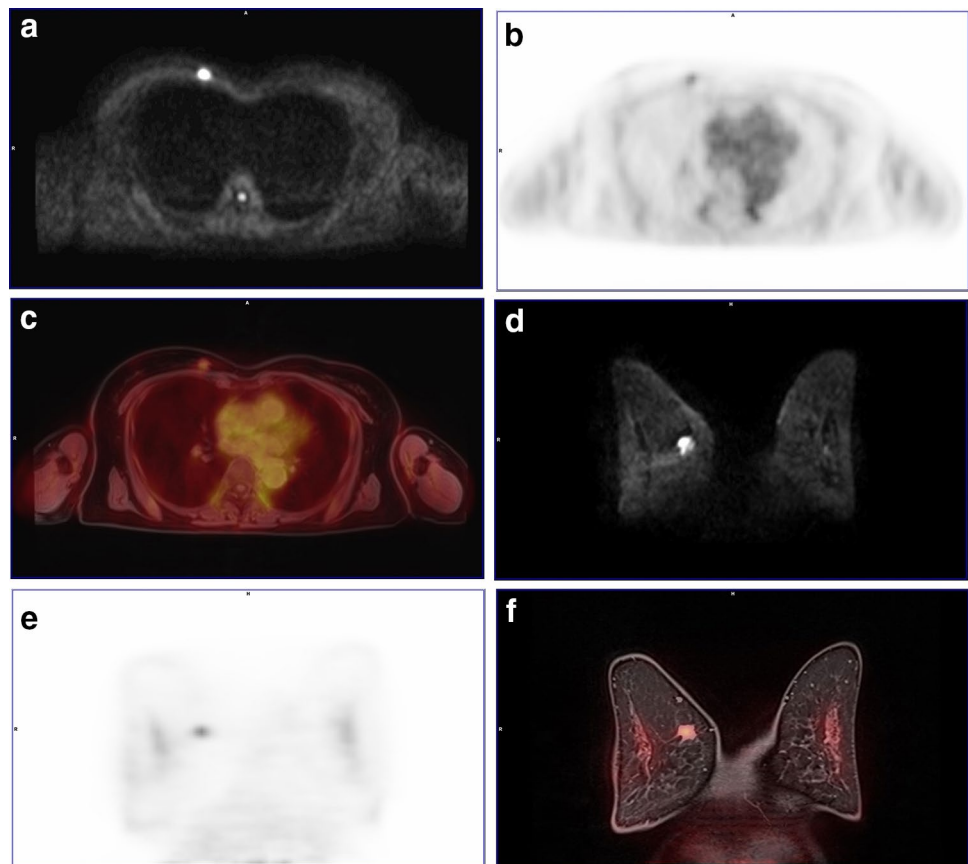




**Table 3** Characteristics of lesions with negative findings on diffusion-weighted imaging and PET imaging

Histopathology	No. of lesions on DWI ( <i>N</i> = 13)	No. of lesions on PET ( <i>N</i> = 7)
Scirrhous carcinoma	3	5
Papillotubular carcinoma	2	1
Solid-tubular carcinoma	1	
Invasive lobular carcinoma	1	
DCIS	6	1

was 13% (5/40), and the average size of these lesions was 14.0 mm (range: 8–22 mm). Two patients had DCIS lesions that were diagnosed as encapsulated papillary carcinoma

(Fig. 2); both of these lesions had a high SUVmax (SUVmax = 7.63 and 10.14, respectively).

Thirteen lesions (13%) were difficult to identify visually using whole-body DWI, and their ADCs could not be determined (Table 2). These lesions included DCIS in 6 lesions, scirrhous carcinoma in 3 (Fig. 3), papillotubular carcinoma in 2, solid-tubular carcinoma in 1, and invasive lobular carcinoma in 1 (Table 3). The average size of these 13 lesions was 29.3 mm (range: 5–80 mm). The proportion of scirrhous carcinoma was 8% (3/40), and the average size of these lesions was 23.3 mm (range: 8–40 mm). The anatomic sites of the lesions were the upper quadrants in 7 patients, the lower quadrants in 5, and directly subjacent to the nipple in 1 patient; hence, no characteristic findings were observed in this respect.

**Fig. 2** Whole-body PET/MR images of a 76-year-old patient with encapsulated papillary carcinoma of the left breast. High SUVmax value (10.14) was noted in this case (a, c). Fusion of PET data and water-weighted Dixon MR data (axial and coronal images) acquired on hybrid PET/MR (b, d)

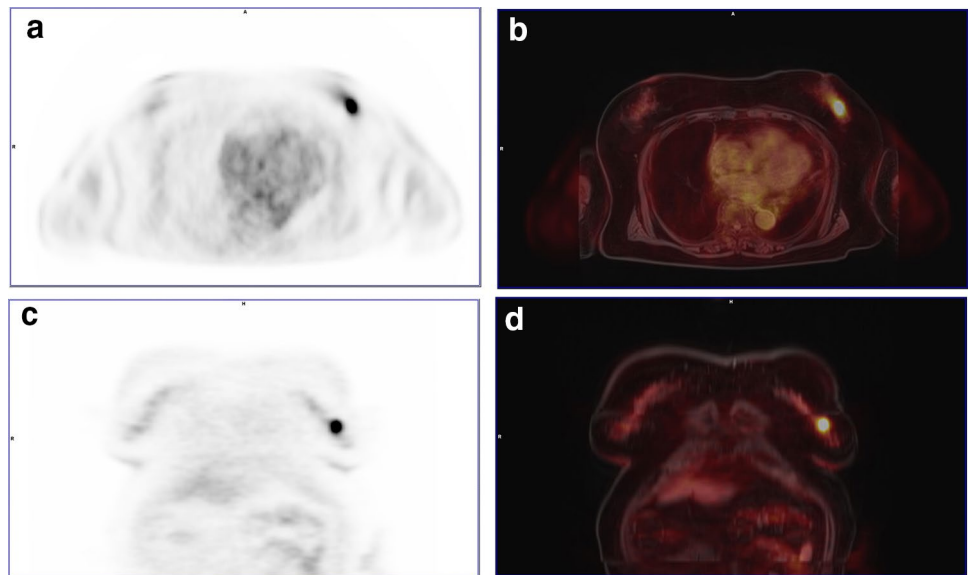
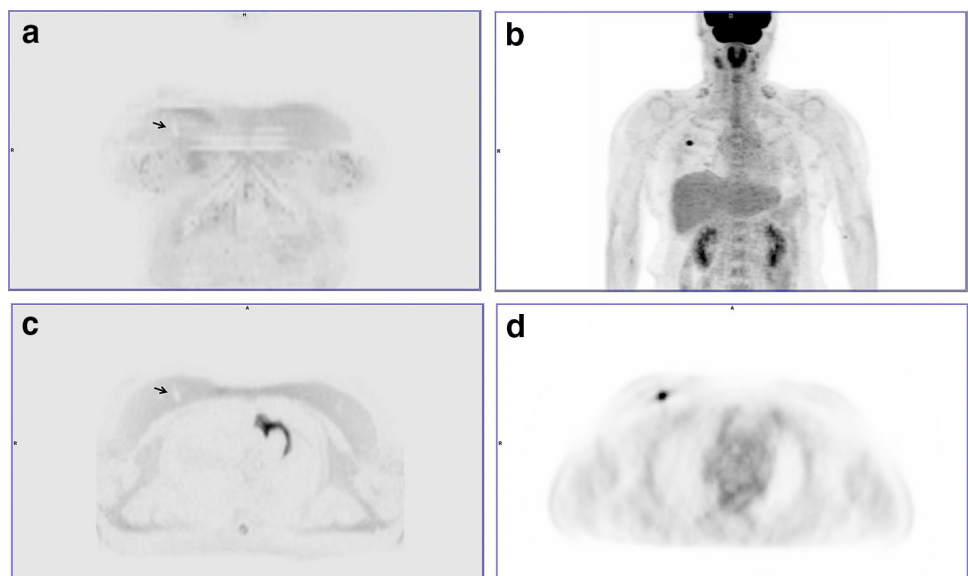


**Fig. 3** Whole-body PET/MR images of a 43-year-old patient with invasive ductal carcinoma of the right breast. Inverted gray scale axial and coronal DWI could not depict the right breast tumor (arrow) (a, c), but PET images show that the lesion is associated with a focal uptake of  $^{18}\text{F}$ -FDG (b, d)



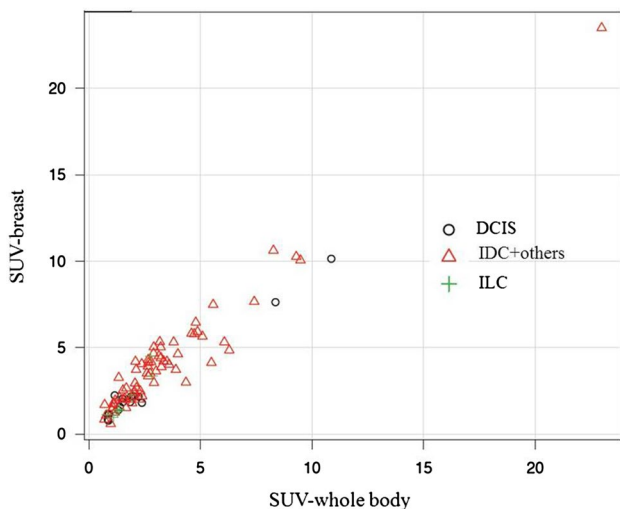
### Relationship between DWI and PET imaging

A strong correlation was noted between the SUV-whole body and SUV-breast findings ( $\rho = 0.928, p < 0.001$ ) (Fig. 4). A moderate correlation was also evident between the ADC-whole body and ADC-breast findings ( $\rho = 0.613, p < 0.001$ ) (Fig. 5). Meanwhile, an analysis of the breast PET/MRI data failed to show any significant correlation between the ADC and SUV findings (Fig. 6).

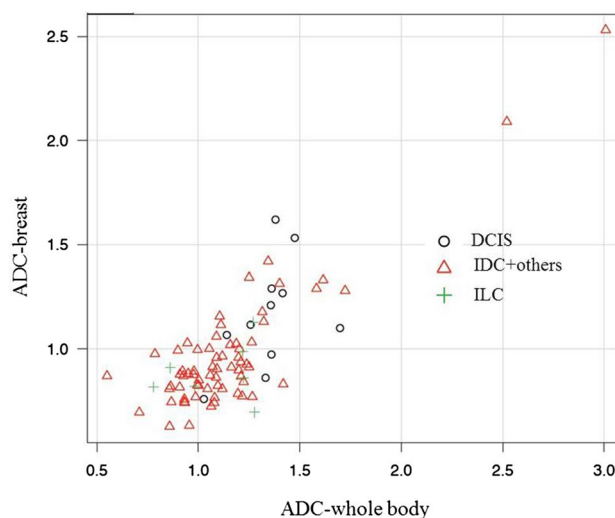
### Histopathological correlations

Table 4 shows the mean ADC value and SUVmax of the 100 mass lesions observed using breast PET/MRI. In a univariate analysis, SUVmax was significantly correlated with the HER2 status ( $p < 0.001$ ), Ki-67 ( $p = 0.014$ ), tumor size ( $p = 0.0177$ ), and nuclear grade ( $p = 0.0448$ ). In contrast, ADCmean was significantly associated with the nuclear grade only ( $p = 0.00399$ ). Neither ADCmean nor SUVmax were significantly associated with the ER and PgR status, or the lymph node status ( $p > 0.05$ ).

Multiple regression analysis was performed to select independent clinicopathological variables associated with SUVmax or ADCmean for all patients with primary breast carcinoma. The variables entered into the multivariate models included tumor size (categorized as  $\leq 20$  mm versus  $> 20$  mm), nuclear grade (categorized as grade 1 versus grade 2 or 3), ER, PR, HER2, and Ki-67 expression (categorized as  $< 14\%$  versus  $\geq 14\%$ ), and axillary nodal status.



**Fig. 4** SUV-based evaluation of the correlation of  $^{18}\text{F}$ -FDG uptake between whole-body PET/MR and subsequent breast PET/MR in breast cancer. The x-axis displays quantitative values obtained by whole body PET/MR, and the y-axis displays the corresponding values obtained by breast PET/MR. A strong and highly significant correlation is found between SUV-whole body and SUV-breast ( $\rho = 0.928, p < 0.001$ )



**Fig. 5** A moderate correlation was evident between the ADC-whole body and ADC-breast findings ( $\rho = 0.613, p < 0.001$ )

Whereas nuclear grade ( $p = 0.00157$ ) and Ki-67 expression ( $p = 0.0149$ ) were shown to independently influence ADCmean, only tumor size ( $p = 0.00701$ ) was shown to independently influence SUVmax (Table 5).

Table 6 shows ROC analysis for breast lesions with corresponding areas under curve (AUC) for SUVmax and ADCmean. Based on these data, the best cutoff values of SUVmax for tumor size was found to be 2.670 (sensitivity 0.800, specificity 0.525). On the other hand, the best cutoff values of ADCmean for nuclear grade and Ki-67 expression was found to be 0.914 (sensitivity 0.771, specificity 0.543) and 0.904 (sensitivity 0.568, specificity 0.500), respectively. The comparison of AUCs revealed that the only statistically

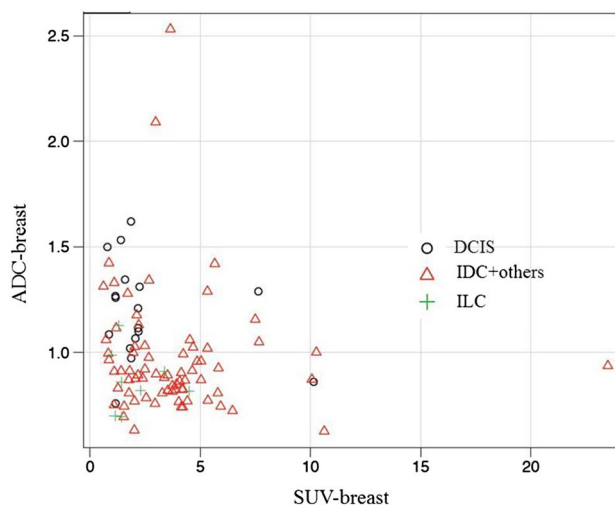


**Fig. 6** An analysis of the breast PET/MRI data failed to show any significant correlation between the ADC-breast and SUV-breast findings

**Table 4** Association between tumor status and tumor SUVmax and ADCmean in breast PET/MRI

Factor	No. of lesions	Median SUVmax (range)	<i>P</i> value	Median ADC × 10 <sup>-3</sup> mm <sup>2</sup> /s (range)	<i>P</i> value
Tumor size					
≤ 20 mm	60	3.02 (0.60–7.66)	0.0177	0.955 (0.632–2.532)	0.581
> 20 mm	23	5.36 (1.08–23.49)		1.015 (0.627–2.091)	
DCIS	17				
ER					
Positive	77	3.69 (0.60–23.49)	0.63	0.978 (0.627–2.532)	0.63
Negative	6	3.47 (2.48–4.67)		0.889 (0.741–1.032)	
DCIS	17				
PgR					
Positive	66	3.84 (0.60–23.49)	0.241	0.987 (0.627–2.532)	0.696
Negative	17	3.01 (0.72–7.66)		0.911 (0.695–1.116)	
DCIS	17				
HER2 receptor					
Positive	8	5.66 (1.26–10.06)	< 0.001	0.934 (0.724–1.420)	0.647
Negative	76	3.37 (0.60–23.49)		0.990 (0.627–2.532)	
N/A	16				
Nuclear grade					
1	47	3.58 (0.60–23.49)	0.0448	0.986 (0.627–2.532)	0.00399
2+3	36	4.43 (2.01–10.26)		0.856 (0.741–1.050)	
DCIS	17				
Ki-67					
< 14%	44	3.01 (0.72–10.62)	0.014	0.972 (0.627–2.532)	0.851
≥ 14%	39	4.42 (0.60–23.49)		0.971 (0.724–2.091)	
N/A	17				
Axillary lymph node metastasis					
Positive	20	4.31 (1.41–9.48)	0.0664	0.909 (0.627–1.979)	0.131
Negative	62	3.44 (0.60–23.49)		0.970 (0.632–2.091)	
N/A	1				
DCIS	17				

N/A Not available

significant cutoff was for the HER2 receptor (AUC 0.789, cutoff value 4.130, sensitivity 0.875, specificity 0.703). There was no statistically significant finding using the AUC based on SUVmax and ADCmean for other factors.

## Discussion

For all 100 breast lesions in the present series, the target lesion was visualized using DWI as well as PET. An analysis of the ADC and SUV data demonstrated a statistically significant correlation between whole-body imaging and breast imaging ( $\rho = 0.613$ ,  $p < 0.001$  and  $\rho = 0.928$ ,  $p < 0.001$ , respectively). As the SUV, in particular, tended to be less dispersed, SUV-whole body imaging may be substituted, to some extent, for SUV-breast imaging. In the whole-body PET/MRI study, however, lesions were visually undetectable on DWI in 13 patients (13%) or on PET in 7 patients

(7%); consequently, neither the ADC nor the SUV could be determined in these cases. Prone breast imaging was more sensitive than whole-body PET/MRI for the detection of breast cancers.

Kong et al. [4] visually examined the breast cancer detection rates using whole-body imaging and breast imaging and reported that the tumors could not be visualized using either modality in 10.4% (5/48) of the cases. Their visualization failure rate using whole-body PET/MRI was similar to the pertinent data reported in the present study. However, the lesions could be visualized using breast PET/MRI in all of the cases in the present study. The success in the present series may be ascribed, at least in part, to the acquisition of images with minimal shifts thanks to the use of contrast-enhanced MRI as a reference for the measurement and also to the simultaneous acquisition of MRI and PET information with the same positioning. This benefit represents an advantage of hybrid PET/MR and is a requirement for accurate



**Table 5** Multiple regression analysis showing the effect of different characteristics on SUV max and ADC mean

	Favorable	Unfavorable	<i>p</i> value	<i>t</i> value
SUV max				
Tumor size	≤ 20 mm	> 20 mm	0.00701*	2.780
ER	Positive	Negative	0.67873	0.416
PgR	Positive	Negative	0.73722	0.337
HER2 receptor	Negative	Positive	0.37682	0.890
Nuclear grade	1	2 + 3	0.63478	- 0.477
Ki-67 index status	< 14%	≥ 14%	0.10541	1.641
Axillary lymph node metastasis	Negative	Positive	0.6806	0.413
ADC mean				
Tumor size	≤ 20 mm	> 20 mm	0.09597	1.688
ER	Positive	Negative	0.42639	0.800
PgR	Positive	Negative	0.64162	- 0.467
HER2 receptor	Negative	Positive	0.7062	0.379
Nuclear grade	1	2+3	0.00157*	- 3,293
Ki-67 index status	< 14%	≥ 14%	0.0149*	2.497
Axillary lymph node metastasis	Negative	Positive	0.16262	- 1.411

\* *p*<0.05

**Table 6** Receiver operating characteristic ( ROC ) analysis

	AUC (95% CI)	Cutoff values	Sensitivity	Specificity
SUV max				
Tumor size	0.676 (0.534–0.818)	2.670	0.800	0.525
ER	0.558 (0.384–0.732)	2.380	0.505	0.857
PgR	0.577 (0.447–0.706)	2.670	0.526	0.682
HER2 receptor	0.789 (0.590–0.988)	4.130	0.875	0.703
Ki-67 index status	0.651(0.531–0.772)	3.730	0.568	0.682
Axillary lymph node metastasis	0.688 (0.568–0.808)	3.510	0.737	0.675
Nuclear grade	0.620 (0.497–0.742)	2.380	0.743	0.478
ADC mean				
Tumor size	0.495 (0.343–0.647)	0.898	0.600	0.541
ER	0.547(0.327–0.767)	0.904	0.560	0.571
PgR	0.540 (0.407–0.673)	0.958	0.579	0.545
HER2 receptor	0.540 (0.315–0.764)	0.904	0.625	0.500
Ki-67 index status	0.490 (0.362–0.618)	0.904	0.568	0.500
Axillary lymph node metastasis	0.696 (0.582–0.810)	0.926	0.842	0.532
Nuclear grade	0.677(0.561–0.793)	0.914	0.771	0.543

AUC Areas under the curve, CI confidence interval

ADC vs SUV comparisons. Another reason may lie in the single-step high resolution imaging and data acquisition time. According to the present protocol, the imaging times for DWI were 2 min for whole-body imaging and 3 min for breast imaging, while the PET acquisition time was 4 min for whole-body imaging and 15 min for breast imaging.

In the present study, the mean lesion size among the 7 patients with failed visualization on whole-body PET was 19.3 mm (5–60 mm), including 3 patients whose lesions measured ≤ 10 mm. The lesions were nuclear grade 1 in 5 patients, nuclear grade 2 in 1 patient, and intermediate in 1

patient with DCIS. In addition, the proportion of scirrhous carcinoma was 13% (5/40). Kumar et al. concluded in their report that a lesion size of ≤ 10 mm and a low-grade tumor were strong predictors of false-negative findings [29]. The results of a study reported by Avril et al. showed a low detection sensitivity for lesions measuring ≤ 10 mm [30].

Avril et al. reported that false-negative imaging findings were obtained in 65.2% of patients with invasive lobular carcinoma, which was higher than the percentage in patients with invasive ductal carcinoma (23.7%) [30]. They assumed that the detection failure might be attributable to the low

tumor cell density in the absence of any noticeable difference in the diameter of invasion [30]. Invasive lobular carcinoma was detected in all 8 patients in the present study, none of which were small lesions measuring  $\leq 10$  mm in diameter, and all the patients were elderly (average of 64 years old) with smaller amounts of normal mammary gland tissues, thereby making tumor detection easier. In 1 patient in her 40s whose mammary glands remained relatively intact, however, the successful identification of the lesion using contrast-enhanced MRI was thought to have enabled the detection of the lesion using PET. This case illustrates the advantage of the simultaneous acquisition of data using whole-body PET/MR. In the study reported by Avril et al., the evaluation was performed separately using conventional image reading (CIR) and sensitive image reading (SIR) [30]. The CIR results were obtained by regarding only the focal tracer accumulation of tracer (grade 3) as representing malignancy, and the SIR was achieved by including probable (grade 2) and definite (grade 3) malignant lesions. Meanwhile, the evaluation used in the present study was performed in a manner similar to that of the SIR, with diffuse or moderate focal increases in FDG uptake (grade 2) and focally marked increased FDG uptake (grade 3) regarded as positive findings, and this strategy might have increased the detection sensitivity.

The detection sensitivity for DCIS with PET was as high as 94.1% (16/17) in our study. A detection sensitivity of 53.8% (28/52) was reported by Fujioka et al., in which the findings were interpreted as positive when the tomographic scans revealed a greater emission than the surrounding normal tissues [31]. The detection sensitivity for DCIS with PET varies from report to report, with a sensitivity of 75% (51/68) reported by Yoon et al. [32] and a sensitivity of 25% (3/12) reported by Avril et al. [30]. It seems reasonable to infer that biopsy-associated inflammatory changes might have influenced the high detection sensitivity observed in the present study. The involvement of encapsulated papillary carcinoma in DCIS was evident in 2 patients. High SUV<sub>max</sub> values were noted in both of these cases (SUV<sub>max</sub> = 7.63 and 10.14). This finding may need to be further examined, since no report has ever dealt with the relation between encapsulated papillary carcinoma and a high SUV.

The accuracy of whole-body DWI in this study was 87% (87/100), which was not satisfactory. This accuracy was similar to that of the diagnostic staging for breast cancer reported by Catalano et al. (PET/CT: 75%, whole-body DWI: 84%, PET/MRI: 98%) [9]. The sizes of the undetectable lesions in 13 patients in the present study averaged 29.3 mm and ranged up to 80 mm. An investigation of the association between undetectable lesions and their locations did not reveal any characteristic findings with regard to the site of the neoplasms (upper quadrants in 7 patients, lower quadrants in 5 patients, and directly subjacent to the nipple

in 1 patient). Among these 13 patients, DCIS was the most frequent type, occurring in 6 patients (46%), of whom 4 patients had Van Nuys grade 2 and 3 lesions, whereas low-grade DCIS was rather infrequent. These results suggest that the accuracy of the whole-body DWI method that was used was a limitation of this study. Unsolved problems include the heterogeneity of the magnetic field resulting from effects such as the shape of the neck and the presence of air in the lung field during whole-body imaging and the likelihood of artifacts and coil sensitivity unevenness in the step border because of respiratory movements. Further improvement in the precision of these imaging methods is anticipated.

There was no evidence of a correlation between ADC-breast and SUV-breast in the present study. Three out of 6 reports on the correlation between these two parameters have demonstrated a modest association, while the other three papers did not show an appreciable association [19–24]. In univariate analysis, regarding the association between PET findings and pathologic findings, our results were roughly consistent with the above-mentioned papers. SUV<sub>max</sub> is reportedly correlated with many prognostic factors, such as tumor size, ER, PgR, Her2, Ki-67, nuclear grade, axillary lymph node metastasis, and TMN stage [19–24], and this trend was similar to our results (HER2 status:  $p < 0.001$ , Ki-67:  $p = 0.014$ , tumor size:  $p = 0.0177$ , and nuclear grade:  $p = 0.0448$ ). Regarding ADC, on the other hand, no evidence of an association with the hormonal expression status was seen according to 3 [19, 20, 22] out of 5 papers dealing with this topic [19–23], while the other 2 papers purported to demonstrate an association [21, 23]. Our results showed an association with nuclear grade alone, although no other reports have documented such an association. Multiple regression analysis showed that nuclear grade ( $p = 0.00157$ ) and Ki-67 expression ( $p = 0.0149$ ) were shown to independently influence ADC<sub>mean</sub>. Meanwhile, only tumor size ( $p = 0.00701$ ) was shown to independently influence SUV<sub>max</sub>. Furthermore, the comparison of AUCs based on SUV<sub>max</sub> revealed that there was statistical significance in the AUC for only HER2 receptor. The differences among statistical analyses seemed to be caused by a small number of cases; however, the pathologic relationship depicted by two types of examinations, i.e., ADC-breast and SUV-breast, might differ from each other. The association between ADC and prognostic factors, compared with SUV, is likely to remain a topic of great debate. In view of the relatively small sample size in this study, we hope to perform even more precise pathologic investigations after the further accumulation of clinical cases.

Our study had several limitations. The first is that only one radiologist performed SUV and ADC measurements; hence, the reproducibility of the pertinent data is a concern. Also, this investigation was not performed as a blinded prospective study, but as a retrospective study conducted with

knowledge of other relevant imaging and clinical information available at the time of image interpretation and evaluation. Thus, a possible bias must be taken into account. Highly reproducible prospective studies using a defined set of criteria for size and location of the ROI are needed in the future. In addition, the relationship between PET and ADC parameter should be examined between SUV<sub>mean</sub> whose area corresponds to that of ADC<sub>mean</sub>. Finally, the number of lesions included in this study ( $n = 100$ ) was relatively small. Also, it may be necessary to align tumor size. Further study comparing highly precise SUV and ADC data after the accumulation of a larger number of clinical cases is needed.

### Compliance with ethical standards

**Conflict of interest** The authors declare that they have no conflict of interest.

### References

- Grueneisen J, Sawicki LM, Wetter A, Kirchner J, Kinner S, Aktas B, et al. Evaluation of PET and MR datasets in integrated <sup>18</sup>F-FDG PET/MRI: a comparison of different MR sequences for whole-body restaging of breast cancer patients. *Eur J Radiol.* 2017;89:14–9.
- Taneja S, Jena A, Goel R, Sarin R, Kaul S. Simultaneous whole-body F-FDG PET-MRI in primary staging of breast cancer: a pilot study. *Eur J Radiol.* 2014;83:2231–9.
- Botsikas D, Kalovidouri A, Becker M, Copercini M, Djema DA, Bodmer A, et al. Clinical utility of <sup>18</sup>F-FDG-PET/MR for preoperative breast cancer staging. *Eur Radiol.* 2016;26:2297–307.
- Kong EJ, Chun KA, Bom HS, Lee J, Lee SJ, Cho IH. Initial experience of integrated PET/MR mammography in patients with invasive ductal carcinoma. *Hell J Nucl Med.* 2014;17:171–6.
- Wehner J, Weissler B, Dueppenbecker PM, Gebhardt P, Goldschmidt B, Schug D, et al. MR-compatibility assessment of the first preclinical PET-MRI insert equipped with digital silicon photomultipliers. *Phys Med Biol.* 2015;60:2231–55.
- Delso G, Fürst S, Jakoby B, Ladeback R, Ganter C, Nekolla SG, et al. Performance measurements of the Siemens mMR integrated whole-body PET/MR scanner. *J Nucl Med.* 2011;52:1914–22.
- Delso G, Ziegler S. PET/MRI system design. *Eur J Nucl Med Mol Imaging.* 2009;36:S86–92.
- Yoon HS, Ko GB, Kwon SL, Lee CM, Ito M, Chan Song I, et al. Initial results of simultaneous PET/MRI experiments with an MRI-compatible silicon photomultiplier PET scanner. *J Nucl Med.* 2012;53:608–14.
- Catalano OA, Daye D, Signore A, Iannace C, Vangel M, Luongo A, et al. Staging performance of whole-body DWI, PET/CT and PET/MRI in invasive ductal carcinoma of the breast. *International J Oncology.* 2017;51:281–8.
- Catalano OA, Rosen BR, Sahani DV, Hahn PF, Guimaraes AR, Vangel MG, et al. Clinical impact of PET/MR imaging in patients with cancer undergoing same-day PET/CT: initial experience in 134 patients—a hypothesis-generating exploratory study. *Radiology.* 2013;269:857–69.
- Pace L, Nicolai E, Luongo A, Aiello M, Catalano OA, Soricelli A, et al. Comparison of whole-body PET/CT and PET/MRI in breast cancer patients: lesion detection and quantitation of <sup>18</sup>F-deoxyglucose uptake in lesions and in normal organ tissues. *Eur J Radiol.* 2014;83:289–96.
- Melsaether AN, Raad RA, Pujara AC, Ponzo FD, Pysarenko KM, Jhaveri K, et al. Comparison of whole-body <sup>18</sup>F FDG PET/MR imaging and whole-body <sup>18</sup>F FDG PET/CT in terms of lesion detection and radiation dose in patients with breast cancer. *Radiology.* 2016;281:193–202.
- Albano D, Patii C, La Grutta L, Agenello F, Grassettonio E, Mulè A, et al. Comparison between whole-body MRI with diffusion-weighted imaging and PET/CT in staging newly diagnosed FDG-avid lymphomas. *Eur J Radiol.* 2016;85:313–8.
- Jambor I, Kuisma A, Ramadan S, Huovinen R, Sandell M, Kajander S, et al. Prospective evaluation of planar bone scintigraphy, SPECT, SPECT/CT, <sup>18</sup>F-NAF PET/CT and whole body 1.5T MRI, including DWI, for the detection of bone metastasis in high risk breast and prostate cancer patients: SKELETA clinical trial. *Acta Oncol.* 2016;55:59–67.
- Tozaki M, Fukuma E. 1H MR spectroscopy and diffusion-weighted imaging of the breast: are they useful tools for characterizing breast lesions before biopsy? *AJR Am J Roentgenol.* 2009;193:840–9.
- Ma D, Lu F, Zou X, Zhang H, Li Y, Zhang L, et al. Intravoxel incoherent motion diffusion-weighted imaging as an adjunct to dynamic contrast-enhanced MRI to improve accuracy of the differential diagnosis of benign and malignant breast lesions. *Magn Reson Imaging.* 2017;36:175–9.
- Dijkstra H, Dorrius MD, Wielema M, Pijnappel RM, Qudkerk M, Sijens PE. Quantitative DWI implemented after DCE-MRI yields increased specificity for BI-RADS 3 and 4 breast lesions. *J Magn Reson Imaging.* 2016;44:1642–9.
- Partridge SC, DeMartini WB, Kurland BF, Eby PR, White SW, Lehman CD. Quantitative diffusion-weighted imaging as an adjunct to conventional breast MRI for improved positive predictive value. *AJR Am J Roentgenol.* 2009;193:1716–22.
- Kitajima K, Yamano T, Fukushima K, Miyoshi Y, Hirota S, Kawanaka Y, et al. Correlation of the SUV<sub>max</sub> of FDG-PET and ADC values of diffusion-weighted MR imaging with pathologic prognostic factors in breast carcinoma. *Eur J Radiol.* 2016;85:943–9.
- Nakajo M, Kajijiya Y, Kaneko T, Takasaki T, Tani A, Ueno M, et al. FDG PET/CT and diffusion-weighted imaging for breast cancer: prognostic value of maximum standardized uptake values and apparent diffusion coefficient values of the primary lesion. *Eur J Nucl Med Mol Imaging.* 2010;37:2011–20.
- Choi BB, Kim SH, Kang BJ, Lee JH, Song BJ, Jeong SH, et al. Diffusion-weighted imaging and FDG PET/CT: predicting the prognoses with apparent diffusion coefficient values and maximum standardized uptake values in patients with invasive ductal carcinoma. *World J Surg Oncol.* 2012;10:126.
- Karan B, Pourbagher A, Torun N. Diffusion-weighted imaging and <sup>18</sup>F-fluorodeoxyglucose positron emission tomography/computed tomography in breast cancer: correlation of the apparent diffusion coefficient and maximum standardized uptake values with prognostic factors. *J Magn Reson Imaging.* 2016;43:1436–44.
- Baba S, Isoda T, Maruoka Y, Kitamura Y, Sasaki M, Yoshida T, et al. Diagnostic and prognostic value of pretreatment SUV in <sup>18</sup>F-FDG/PET in breast cancer: comparison with apparent diffusion coefficient from diffusion-weighted MR imaging. *J Nucl Med.* 2014;55:736–42.
- Byun BH, Noh WC, Lim I, Lee SS, Cho AR, Park JA, et al. A new method for apparent diffusion coefficient measurement using sequential <sup>18</sup>F-FDG PET and MRI: correlation with histological grade of invasive ductal carcinoma of the breast. *Ann Nucl Med.* 2013;27:720–8.
- Martinez-Moller A, Souvatzoglou M, Delso G, Bundschuh RA, Chefd'hotel C, Ziegler SI, et al. Tissue classification as a potential

- approach for attenuation correction in whole-body PET/MRI: evaluation with PET/CT data. *J Nucl Med.* 2009;50:520–6.
26. Martinez-Moller A, Eiber M, Nekolla SG, Souvatzoglou M, Drzezga A, Ziegler S, et al. Workflow and scan protocol considerations for integrated whole-body PET/MRI in oncology. *J Nucl Med.* 2012;53:1415–26.
  27. American College of Radiology. Breast imaging reporting and data system: breast imaging atlas (BI-RADS). 5th ed. Reston Va: ACR; 2013.
  28. Kanda Y. Investigation of the freely available easy-to-use software 'EZR' for medical statistics. *Bone Marrow Transplant.* 2013;48:452–8.
  29. Kumar R, Chauhan A, Zhuang H, Chandra P, Schnall M, Alavi A. Clinicopathologic factors associated with false negative FDG-PET in primary breast cancer. *Breast Cancer Res Treat.* 2006;98:267–74.
  30. Avril BN, Rosé CA, Shelling RM, Dose J, Kuhn W, Bense S, et al. Breast imaging with positron emission tomography and fluorine-18 fluorodeoxyglucose: use and limitations. *J Clin Oncol.* 2000;18:3495–502.
  31. Fujioka T, Kubota K, Toriihama A, Machida Y, Okazawa K, Nakagawa T, et al. Tumor characteristics of ductal carcinoma in situ of breast visualized on [F-18] fluorodeoxyglucose-positron emission tomography/computed tomography: results from a retrospective study. *World J Radiol.* 2016;8:743–9.
  32. Yoon HJ, Kim Y, Kim BS. Intratumoral metabolic heterogeneity predicts invasive components in breast ductal carcinoma in situ. *Eur Radiol.* 2015;25:3648–58.